Surv Geophys (2017) 38:727–755
DOI 10.1007/s10712-017-9415-5

An Overview of Fe—Mg Interdiffusion in Mantle Minerals

Baohua Zhang[1]

Received: 1 January 2017 / Accepted: 28 April 2017 / Published online: 17 May 2017
© Springer Science+Business Media Dordrecht 2017

Abstract The rates of Fe–Mg interdiffusion in the Earth's materials are of fundamental importance to a wide range of geochemistry and geophysics problems. In order that the Earth Scientist may readily apply the available experimentally determined diffusion rates to such problems, a brief review of experimental data for Fe–Mg interdiffusion in mantle minerals is presented concerning new advances and some recent applications. Perspectives for the future are also suggested.

Keywords High temperature and high pressure · Mantle mineral · Fe–Mg interdiffusion · Point defects

1 Introduction

Diffusion in solids is an important topic of materials science, physical metallurgy, materials science, geosciences and many other areas. Solid-state diffusion of cations in silicate minerals has been recognized to play a fundamental role in numerous geodynamical, petrological and geochemical processes involving mass transport (Ganguly 2002; Watson and Baxter 2007; Chakraborty 2008; Brady and Cherniak 2010). Hence, knowledge of diffusion coefficients allows constraints to be placed upon timescales and thermodynamic conditions in many natural contexts where mass transport is dominated by solid-state diffusive processes.

Fe and Mg are very important elements in the Earth and terrestrial planets. Study of the rates of Fe–Mg interdiffusion in silicate minerals is clearly of fundamental importance in enhancing our understanding of geological and planetary processes. For instance, Fe–Mg interdiffusion in silicate minerals is of interest in petrological studies for determining the

✉ Baohua Zhang
zhangbaohua@vip.gyig.ac.cn

[1] Key Laboratory for High-Temperature and High-Pressure Study of the Earth's Interior, Institute of Geochemistry, Chinese Academy of Sciences, Guiyang 550081, China

closure temperature of geothermometers and for determining timescales of various processes such as magma ascent, magma mixing, cooling of lava flows, volcano eruption and tectono-metamorphic event (e.g., Ganguly and Tirone 1999; Ganguly 2002; Chakraborty 2008; Borinski et al. 2012; Müller et al. 2013; Dohmen et al. 2016). It is also relevant for studies of many physical and chemical problems in the Earth's interior, such as rheology (Demouchy et al. 2007), chemical heterogeneities (Chakraborty et al. 1999; Yamazaki and Irifune 2003; Holzapfel et al. 2005, 2009), electrical conductivity (Farber et al. 2000; Hier-Majumder et al. 2005; Otsuka and Karato 2015), *P–T–t* paths of metamorphic rocks (Ganguly 2002; Chakraborty 2008), thermal history (cooling rate) of terrestrial ultramafic rocks (Liermann and Ganguly 2002), reaction mechanisms of minerals (Ganguly and Tazzoli 1994).

Very considerable efforts have been directed toward the determination of more accurate diffusion coefficients for a wide range of elements in a wider range of minerals, together with the new experimental tools that are just becoming available (including high-pressure techniques and analytical tools). To date, a significant body of experimental diffusion data now exists in the literature, and partial reviews for systems and materials of geological interest are available (Freer 1981; Brady 1995; Ganguly 2002; Béjina et al. 2003; Watson and Baxter 2007; Chakraborty 2008, 2010; Brady and Cherniak 2010; Cherniak and Dimanov 2010). All of these treatments are based on the same general concepts of diffusion, which do not need restating here in great detail. This review mainly focuses on a compilation of fairly new advances in experimental laboratory work on Fe–Mg interdiffusion in mantle minerals, starting with a simple introduction about fundamentals of diffusion and experimental techniques and then following by discussions about the available data and its applications. Finally, some suggestions for directions of future development are addressed.

2 Fundamentals of Diffusion and Experimental Measurement Techniques

2.1 Basic Principles of Diffusion

Diffusion is a process by which thermally activated atoms, ions, and molecules in materials are transported from one part of a system to another as a result of random molecular motions (Crank 1975; Zhang 2010). The random motion leads to a net flux when the concentration of a component is not uniform. The initially concentrated atomic species will "diffuse out" as time goes on. Therefore, in a diffusion process, the species tend to diffuse from a highly concentrated region to a less concentrated region, and leads to homogenize the materials.

The equations governing diffusion processes are Fick's laws. The mathematics of the random-walk problem allows us to go back and forth between the diffusion coefficient defined in Fick's laws and the underlying physical quantities of diffusing atoms. This viewpoint is most exciting since it transforms the study of diffusion from the question how a system will homogenize into a tool for studying the atomic processes involved in a variety of reactions in solids. A deeper physical understanding of diffusion in solids is based on random-walk theory and the atomic diffusion mechanism, which are discussed elsewhere (Ganguly 2002; Mehrer 2007; Zhang 2010).

There are many types of diffusion in nature and experimental studies. Because diffusion involves a diffusing species in diffusion medium, it can be classified based on either the

diffusion medium or the diffusing species. When considering the diffusion medium, thermally activated diffusion may be classified as volume diffusion and grain-boundary diffusion. Volume diffusion (also called lattice diffusion) refers to atomic diffusion within a crystalline lattice. In volume diffusion, the diffusion medium can be either isotropic or anisotropic. Both melts (and glasses) and isometric minerals are isotropic diffusion media, but non-isometric minerals are in general anisotropic diffusion media (although in some cases, the dependence of diffusivities on the direction is weak). Grain-boundary diffusion is diffusion along interphase interfaces, including mineral–fluid interfaces (or surfaces), interfaces between the same minerals, and those between different minerals. For example, Fig. 1a illustrates several diffusion pathways in a polycrystalline materials, including diffusion along surface, grain boundaries, crystal lattice, and intergranular boundaries in a rock; or diffusion along subgrain boundaries, dislocations, stacking faults, and linear/planar defect-free crystal lattice in a single crystal. As a consequence, diffusion rates of different elements in the various materials are spread over many orders of magnitude at any given conditions. Figure 1b shows the overall range of log D values versus reciprocal temperature $1/T$ in the complicated Earth materials. It should be noted that the slowest-diffusing species are carbon self-diffusion in graphite and tetravalent ions diffusion in zircon, but their rates are at least lower by 15 orders of magnitude than diffusion in aqueous fluids.

When considering differences in the diffusing species, the diffusion can be classified as self-diffusion, tracer diffusion, interdiffusion coefficient, or chemical diffusion that can be further distinguished as trace element diffusion, binary diffusion, multispecies diffusion, multicomponent diffusion, and effective binary diffusion. It should be pointed out that all of these aspects, in principle, as a function of composition, have been reviewed by Ganguly (2002) and Zhang (2010) in some detail. Chemical interdiffusion coefficient refers to the case of diffusion of two components (A and B) with or without the same charge in a binary system. In general, fluxes of different species are coupled due to constraints of electroneutrality and conservation of lattice sites in a crystal. Chemical interdiffusion coefficient usually varies with concentration (i.e., with distance across the interdiffusion

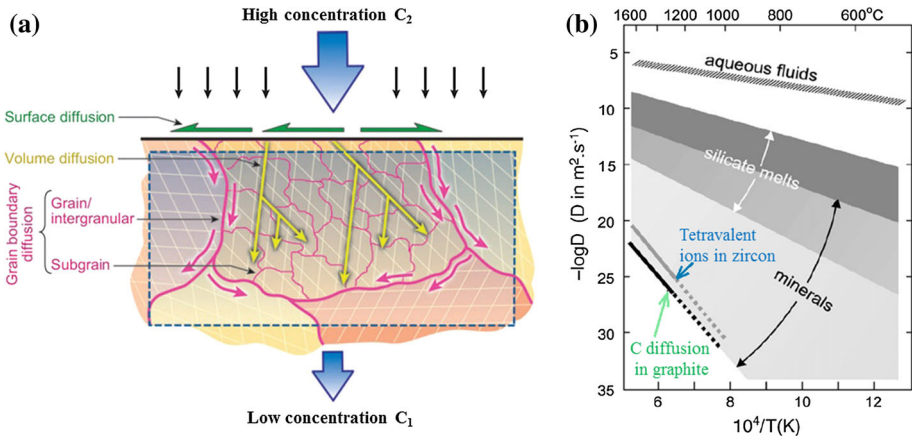

Fig. 1 **a** Schematic drawing various models of diffusion in a polycrystalline material [modified after Chakraborty (2008)]. Three types of diffusion paths (surface, volume and grain boundary) are indicated. **b** Arrhenius plot showing diffusion coefficients in geological materials [modified after Watson and Baxter (2007) and reference therein]

zone) and becomes complicated because interdiffusing species experience thermodynamic effects on top of their intrinsic mobilities, but this can be addressed using the Boltzmann–Matano approach (Shewmon 1963). However, rigorous mathematical treatment of chemical diffusion involves determination of the interdiffusion coefficient has been compiled by Ganguly (2002) and Mehrer (2007).

2.2 Diffusion Mechanism

When the random-walk model is expanded to take into account the real structures of solids, it becomes apparent that diffusion in crystals is dependent upon point defect concentrations. This statement mainly derives from two features: one is the ability of point defects to move through the crystal and to act as "vehicles for diffusion" of atoms; another is their presence at thermal equilibrium. In an ideal (defect-free) crystal, mass and charge density have the periodicity of the lattice. However, the creation of a point defect disturbs this periodicity. Point defects occur only at or around a single lattice point site and are not extended in space in any dimension. Various types of point defects (vacancy, interstitial and substitutional defects) can present thermally in many materials including metal, ionic and molecular crystals (Mehrer 2007; Fei 2013).

Vacancy defects are lattice sites in a crystal which should be occupied by a regular atom or ion, but actually are vacant (Fig. 2). The neighboring atoms or ions could jump into the vacant site, and the vacancy moves in the opposite due to thermal vibration. When cations and anions move to the crystal surface and leave vacancies in their original sites, such cations and anions vacancies are called Schottky defect. Interstitial defects are atoms that occupy a site in the crystal structure at which no atom or ion usually occupies (Fig. 2). When an ion moves into an interstitial site forming a defect pair, a vacancy on the regular site and an interstitial defect, this nearby pair of a vacancy and an interstitial is called a Frenkel defect. Materials in the nature are never 100% pure. Impurity atoms or ions are frequently incorporated into a crystal. This is neither a vacant site nor a regular atom on an

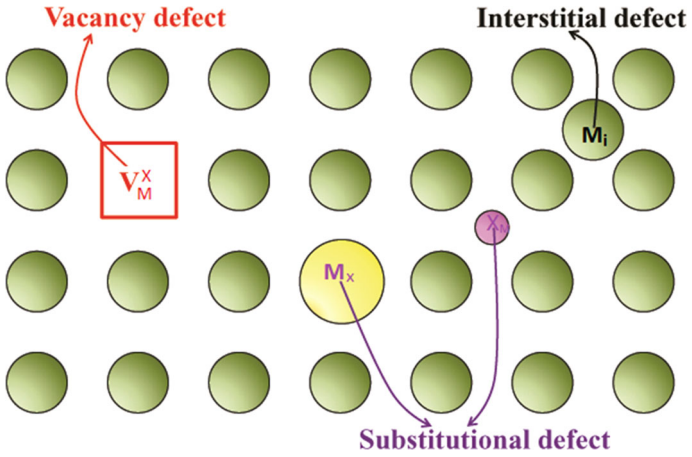

Fig. 2 Vacancy, interstitial and substitutional defects in a crystal. *Different colors* of spheres represent different types of atoms. Note that, V_M^X represents neutral metal (M) vacancy; M_i denotes interstitial metal (M); M_x indicates M atom occupied the position of X atom; X_M is a substitutional atom (X) located in an interstitial site (M)

interstitial site, and it is called a substitutional defect (Fig. 2). The substitutional defects could locate in a regular atomic site or in an interstitial site.

As outlined above the hopping motion of atoms gives rise to diffusion in solids. Therefore, the atomic mechanisms of diffusion in crystalline materials are closely connected with defects. Various atomic mechanisms of diffusion in crystals have been identified and are catalogued: vacancy mechanism, interstitial mechanism, divacancy mechanism, interstitialcy mechanism, interstitial-substitutional exchange mechanism. On the other hand, dislocations, grain/phase boundaries, and free surfaces are other types of defects of crystalline solids. They can act as diffusion short circuits, because the mobility of atoms along such defects is usually much higher than in the lattice. However, by far the most prominent mechanisms among them are the vacancy mechanism and the interstitial mechanism. For more comprehensive understanding of the field of point defects and the diffusion mechanisms in crystals, the reader is referred to the textbooks (e.g., Shewmon 1963; Bokshtein et al. 1985; Borg and Dienes 1988; Chiang et al. 1997; Mehrer 2007; Tilley 2008).

2.3 Dependence of Diffusion on Thermodynamic Variables

In any given diffusion problem, the concentration gradient is controlled by the initial and boundary conditions. Generally speaking, more than one point defect species may be present in a crystal at any temperature, and the amount of matter transported by diffusion will depend upon the number of each defect type present. Therefore, the values of diffusion coefficients in any real system are controlled by thermodynamic intensive variables, such as temperature, pressure, oxygen fugacity, composition, water, the state of strain/deformation, and anisotropy.

2.3.1 Temperature

The atomic jump process is a thermally activated process, and the rate of atomic jump increases significantly with temperature. Thus, the diffusion coefficient, D, depends strongly on temperature. The temperature dependence of diffusion coefficients is generally found to obey the Arrhenius equation:

$$D = D_0 \exp\left(-\frac{\Delta E}{RT}\right) \tag{1}$$

where D is the measured diffusion coefficient, D_0 is a constant term referred to as the pre-exponential factor, ΔE is the activation energy of diffusion, R is the gas constant, and T is the temperature (K). In an Arrhenius diagram, the activation energy can be determined from the gradient of a plot of $\ln D$ versus $1/T$. Diffusion coefficients found in the literature are usually expressed in terms of the Arrhenius equation D_0 and ΔE values. Some representative values for Fe–Mg interdiffusion coefficients are given in Tables 1, 2, 3 and 4.

2.3.2 Pressure

In the view of thermodynamics, pressure could also affect the equilibrium state by influence on the Gibbs free energy and therefore affect the concentration of defects, sequentially affect the diffusion coefficients. A variation of the diffusivity with pressure is

Table 1 Hydrostatic pressure (HP) data on Mg–Fe interdiffusion in Olivine

References	X_{Fe}	T (K)	P (GPa)	LogD_0 (m^2/s)	ΔE (kJ/mol)	ΔV (cm^3/mol)	Remarks
Olivine							
Tachibana et al. (2013)	$0.09 < X_{Fe} < 0.11$	1673–1873	1 atm	−5.02 ± 0.75	315 ± 28		[100], SX, EM
Tachibana et al. (2013)	$0.09 < X_{Fe} < 0.11$	1673–1873	1 atm	−5.86 ± 0.56	280 ± 25		[010], SX, EM
Tachibana et al. (2013)	$0.09 < X_{Fe} < 0.11$	1673–1873	1 atm	−4.29 ± 0.35	323 ± 52		[001], SX, EM
Dohmen et al. (2007)	$0.2 < X_{Fe} < 1.0$	973–1473	1 atm	−9.39	196 ± 12		[100], SX, RBS
Dohmen et al. (2007)	$0.2 < X_{Fe} < 1.0$	973–1473	1 atm	−10.23	191 ± 9		[010], SX, RBS
Dohmen et al. (2007)	$0.2 < X_{Fe} < 1.0$	973–1473	1 atm	−10.16	201 ± 8		[001], SX, RBS
Wang et al. (2004)	$0.09 < X_{Fe} < 0.17$	1373	0.3	−15.94[a]			Wet, SX, EDX-TEM
Jaoul et al. (1995)	$X_{Fe} = 0.10$	873–1173	0.5–9	−11.11 ± 0.18	147 ± 58	0.36–6.5	[010], PC, MA, SX, RBS
Chakraborty (1997)	$X_{Fe} = 0.14$	1253–1573	1 atm	−8.27 ± 0.07	226 ± 18		[001], SX, EM
Chakraborty et al. (1999)	$X_{Fe} = 0.14$	1673	9–12	−14.7 −15.1[a]		0.35	MA, SX, EM
Holzapfel et al. (2007)	$X_{Fe} = 0.06$	1623–1823	12	−5.39 ± 0.65	346 ± 59	5.3 ± 1	[001], SX, EM
Buening and Buseck (1973)	$X_{Fe} = 0.10$	1273–1373		−10.54	117		[001], SX, EM
Misener et al. (1974)	$X_{Fe} = 0.14$	1273–1473	0–3.5	−5.91	242	5.5	[001], PC, SX, EM
Farber et al. (2000)	Mg–Fe	1473	1–3.3			5.4 ± 4	[001], MA, SX, EM
Heir-Majumder et al. (2005)	$0.1 < X_{Fe} < 0.2$	1373–1450	0.1–6	−14.80 ± 2.70	220 ± 60	16 ± 6	Wet, [001], MA, SX, EDS, WDS
Zhang and Shan (2015a)	0.400 ± 0.003	1000–1900	0–14	−3.48 ± 0.07	337 ± 17	(6.06–6.13) ± 0.33	[100], cBΩ model
Zhang and Shan (2015a)	0.364 ± 0.004	1000–1900	0–14	−2.83 ± 0.11	305 ± 21	(5.73–6.51) ± 0.26	[010], cBΩ model
Zhang and Shan (2015a)	0.410 ± 0.005	1000–1900	0–14	−3.04 ± 0.12	343 ± 19	(5.95–6.03) ± 0.12	[001], cBΩ model
Zhang and Shan (2015a)	0.395 ± 0.007	1000–1900	1 atm	−3.59 ± 0.07	329 ± 10		Wet, [001], cBΩ model

PC piston-cylinder; *SX* single crystal; *EM* electron microprobe; *RBS* Rutherford backscattering spectrometry; *SIMS* secondary ion mass spectrometry; *NRA* nuclear reaction analysis; *EDX* energy dispersive X-ray; *TEM* transmission electron microscope; *EDS* energy dispersive spectroscopy; *WDS* wavelength dispersive spectroscopy

[a] Diffusion coefficient was measured only at one temperature, thus no activation energy (ΔE) and pre-exponential factor (D_0) were reported in these studies

Table 2 Hydrostatic pressure (HP) data on Mg–Fe interdiffusion in pyroxene, garnet and spinel

References	X_{Fe}	T (K)	P (GPa)	LogD_0 (m^2/s)	ΔE (kJ/mol)	ΔV (cm^3/mol)	Remarks
Pyroxene							
Dimonav and Sautter (2000)	$X_{Fe} = 0.06$	1173–1513	1 atm	−4.02 ± 0.32	406		SX, RBS, SIMS
Dimonav and Wiedenbeck (2006)	$X_{Fe} = 0.06$	1273–1473	1 atm	−8.47 ± 1.20	297 ± 31		[001], SX, SIMS
Ganguly and Tazzoli (1994)	$0.1 < X_{Fe} < 0.5$	773–1273			240 ± 8		[010], [001]
Müller et al. (2013)	$X_{Fe} = 0.07$	1073–1473	1 atm	−6.56 ± 0.41	321 ± 16		SX, RBS
Dohmen et al. (2016)	$X_{Fe} = 0.01$	1143–1373	1 atm	−3.78 ± 1.26	377 ± 30		[001], SX, RBS
Dohmen et al. (2016)	$X_{Fe} = 0.09$	1143–1373	1 atm	−5.95 ± 0.83	308 ± 23		[001], SX, RBS
Garnet							
Freer and Edwards (1999)	Grs–Alm	1173–1373	1.5–3.3	−5.91 ± 0.79	270 ± 19	11.2 ± 3	PC, SX, EM
Elphick et al. (1985)	Pyr–Alm	1573–1773	2.9–4.3	−9.09	224 ± 20	4.7	PC, SX, EM
Elphick et al. (1985)	Pyr–Alm	1573–1773	2.9–4.3	−8.92	239 ± 35	4.7	PC, SX, EM
Borinski et al. (2012)	Pyr_{60}–Alm_{40}	1273–1673	2.5–3.5	−9.46	232		PC, SX, EM
Spinel							
Freer and O'Reilly (1980)	Her_{25}, $X_{Fe} = 5$ wt%	1073–1307	1 atm	−0.34	334 ± 47		PX, EM
Freer and O'Reilly (1980)	Her_{25}, $X_{Fe} = 25$ wt%	1073–1307	1 atm	−5.96	221 ± 20		PX, EM
Liermann and Ganguly (2002)	Her_{10}	1223–1598	2–3	−7.67	226	5	PC, SX, EM
Vogt et al. (2015)	Her_{50}, $X_{Fe} = 0.001$	1023–1173	1 atm	−7.76 ± 0.90	219 ± 19		SX, RBS
Vogt et al. (2015)	Her_{50}, $X_{Fe} = 0.07$	1023–1173	1 atm	−12.33 ± 0.85	139 ± 18		SX, RBS

PC piston-cylinder; *SX* single crystal; *PX* polycrystal; *EM* electron microprobe; *RBS* Rutherford backscattering spectrometry; *SIMS* secondary ion mass spectrometry; *NRA* nuclear reaction analysis

Table 3 Hydrostatic pressure (HP) data on Mg–Fe interdiffusion in olivine polymorphs

References	X_{Fe}	T (K)	P (GPa)	LogD_0 (m^2/s)	ΔE (kJ/mol)	ΔV (cm^3/mol)	Remarks
Wadsleyite							
Chakraborty et al. (1999)	$0.1 < X_{Fe} < 0.18$	1373–1673	9–15	−9.07	145		MA, PX, EM
Farber et al. (2000)	Mg–Fe	1473	10–14			6.1	MA, SX, EM
Kubo et al. (2004)	$X_{Fe} = 0.03$	1503–1803	16–17	−9.17 ± 0.72	172 ± 23		MA, PX, EM
Kubo et al. (2004)	$X_{Fe} = 0.05$	1503–1803	16–17	−8.91 ± 0.14	172 ± 5		MA, PX, EM
Kubo et al. (2004)	$X_{Fe} = 0.10$	1503–1803	16–17	−8.75 ± 1.75	143 ± 55		MA, PX, EM
Holzapfel et al. (2009)	$X_{Fe} = 0.16$	1373–1773	15	−5.91 ± 1.67	229 ± 27	13.9 ± 1.50	MA, PX, EM
Zhang and Shan (2015a)	Mg–Fe	1000–1900	10–20	−3.61 ± 0.40	289 ± 20	(2.39–3.45) ± 0.02	cBΩ model
Ringwoodite							
Farber et al. (2000)	Mg–Fe	1473	10–14			6.1	MA, PX, EM
Zhang and Shan (2015a)	Mg–Fe	1000–1900	10–24	−2.45 ± 0.08	345 ± 11	(4.90–5.33) ± 0.21	cBΩ model

MA multi-anvil press; *SX* single crystal; *PX* polycrystal; *EM* electron microprobe

Table 4 Hydrostatic pressure (HP) data on Mg–Fe interdiffusion in bridgmanite and ferropericlase

References	X_{Fe}	T (K)	P (GPa)	$\mathrm{Log}D_0$ (m^2/s)	ΔE (kJ/mol)	ΔV (cm^3/mol)	Remarks
Perovskite							
Holzapfel et al. (2005)	$0.02 < X_{Fe} < 0.11$	1973–2273	22–26	−8.40 ± 0.07	414 ± 62	2.1 ± 0.5	f_{O_2} = IW − 3, MA, PX, TEM
Holzapfel et al. (2005)	$0.02 < X_{Fe} < 0.11$	1973–2273	22–26	−7.10 ± 0.07	414 ± 62	2.1 ± 0.5	f_{O_2} = IW + 3, MA, PX, TEM
Zhang and Shan (2015a)	$0.02 < X_{Fe} < 0.11$	1600–2400	0–60	−2.39 ± 0.18	646 ± 22	(4.48–5.61) ± 0.15	cBΩ model
Ferropericlase							
Holzapfel et al. (2003)	$0.07 < X_{Fe} < 0.37$	1653–2073	8–23	−5.01 ± 0.03[a]	255 ± 16[a]	3.3 ± 0.1[a]	SX, MA, EM
Yamazaki and Irifune (2003)	$X_{Fe} = 0.50$	1573–1973	7–35	−6.39	226 ± 32	1.8 ± 1.2	SX, MA, EM
Mackwell et al. (2005)	$0.07 < X_{Fe} < 0.27$	1593–1673	1 atm	−5.54[b]	209[b]		SX, EM
Demouchy et al. (2007)	$0.01 < X_{Fe} < 0.25$	1273–1523	0.3	−3.30[c]	270 ± 20[c]		Wet condition, SX, MA, EM
Otsuka and Karato (2015)	$0.44 < X_{Fe} < 1.0$	1673–1873	5–24	−5.96 ± 0.16	200	2.7 ± 0.2	Wet SX, MA, EM

MA multi-anvil press; *SX* single crystal; *PX* polycrystal; *EM* electron microprobe

[a] All data were fitted at 23 GPa by $D_{Fe-Mg} = D_0 \exp\left(\frac{AX_{FeO}}{RT}\right) \exp\left(-\frac{\Delta E + P\Delta V}{RT}\right)$ with the constant A = 132 ± 13 kJ/mol

[b] All data were fitted by Eq. (4) with $n = 0.19$, $p = 0.73$ and $\alpha = 96$ kJ/mol

[c] All data were fitted by Eq. (4) with $p = 0.8$ and $\alpha = -80$ kJ/mol

largely due to the fact that the Gibbs free energy of activation varies with pressure according to:

$$\Delta G = \Delta H - T\Delta S,\ \Delta H = \Delta E + P\Delta V \tag{2}$$

where ΔG is the Gibbs free energy, ΔH is the activation enthalpy, ΔS is the activation entropy, ΔE is the activation energy, ΔV is the activation volume, which can be either positive (leading to a decrease of D with increasing P) or negative (leading to an increase of D with increasing P). The diffusion coefficient at variable pressure P and temperature T, D (P, T), is then given by:

$$D = D_0 \exp\left(-\frac{\Delta E + P\Delta V}{RT}\right) \tag{3}$$

Although the effect of P on D is small compared to the temperature dependency, but this effect could become significant under the enormous pressure conditions as that in the Earth's interior because pressure can vary widely from the surface to the deep Earth. It is worth noting that, due to the technical difficulties of performing high-pressure diffusion experiments in the laboratory, such pressure dependence has not been investigated well for many systems. This remains an important task for experimentalists in future.

2.3.3 Oxygen Fugacity

In the Earth's interior, most minerals and rocks containing variable valence elements, such as iron, oxygen fugacity (f_{O_2}) is expected to influence the diffusion property by changing the defect concentrations through the change of oxidation state of multivalent element and by changing the defect sites in the structure. For example, the homogeneous redox equilibrium of iron in ferropericlase, (Mg, Fe)O, is governed by the reaction using the Kröger–Vink notation (Ganguly 2002; Zhang 2010):

$$6\mathrm{Fe}_{\mathrm{Fe}}^{\mathrm{X}} + \mathrm{O}_2(\mathrm{gas}) \rightleftharpoons 4\mathrm{Fe}_{\mathrm{Fe}}^{\cdot} + 2\mathrm{FeO} + 2\mathrm{V}_{\mathrm{Fe}}^{''} \tag{4}$$

where x, ´ and · stand for neutral, negative and positive, respectively. V_{Fe} denotes the vacancy in Fe lattice site. Equation (4) suggests the diffusion coefficient is approximately proportional to the 1/6 power of oxygen fugacity. It should be noted that f_{O_2} affects the diffusion coefficient not just of Fe, but also that of other cations. Previous experimental investigations (Chakraborty et al. 1994; Dohmen and Chakraborty 2007) have demonstrated that the dominate diffusion mechanism could change as a function of Fe concentration and f_{O_2}. The vacancy diffusion plays the dominant role at f_{O_2} above the minimum, whereas the interstitial diffusion plays the dominant role at lower f_{O_2}.

2.3.4 Water

Nominally anhydrous minerals (NAMs) of Earth's mantle (olivine and its high-pressure polymorphs, pyroxenes, garnet, etc.) can incorporate "water" as the speciation of H^+, $(OH)^-$ or H_2O, in conjunction with intrinsic point defects in their structure (Kohlstedt et al. 1996; Ingrin and Skogby 2000; Bolfan-Casanova 2005). The presence of water in NAMs, even at very low concentrations, may significantly affect transport properties involving ionic diffusion in minerals. Recent studies have revealed significant enhancement by H_2O of Fe–Mg interdiffusion in olivine (Wang et al. 2004; Hier-Majumder et al. 2005). A similar but smaller effect has also been observed for Fe–Mg interdiffusion in ferropericlase

(Demouchy et al. 2007). In addition, previous Fe–Mg interdiffusion experiments carried out under hydrous conditions indicated that interdiffusivity increases approximately linearly with increasing water fugacity (Wang et al. 2004; Hier-Majumder et al. 2005). The enhancement of diffusion rate has been attributed to the entry of water into the lattice and consequent changes in point defect concentrations (cation vacancies). On the other hand, Cherniak (1993) showed that water may not play a significant role in the interdiffusion process that involves only a simple exchange between cations of the same charge, as well as Ar diffusion in quartz under nominally dry and H_2O-present conditions (Watson and Cherniak 2003). Therefore, it seems that the effect of H_2O on lattice diffusion of cations in deep-seated mantle phases is quite different, perhaps because the available lattice solution mechanisms for H-bearing species are different. So far as we know, the effect of H species on diffusion in crystals is less well understood, but it stands to reason that intracrystalline diffusion can be affected only if H species enter the lattice. However, this topic needs to be carefully investigated in future so the experimental data can be applied to natural systems in a meaningful way.

2.3.5 Composition

The compositional effects on diffusivities are complicated in the Earth materials. For example, Mackwell et al. (2005) performed Fe–Mg interdiffusion experiments in ferropericlase employing single-crystal diffusion couples over a wide range of temperatures, composition and oxygen fugacities at 1 bar. According to their results, diffusion depends on oxygen fugacity with an exponent of 0.22 and depends exponentially on composition. The power law dependence only plays a significant role at low iron concentrations, whereas for compositions with $X_{FeO} > 0.07$, diffusivities are primarily exponentially dependent on composition as indicated in Eq. (4). Similarly, the strong compositional dependence of Fe–Mg interdiffusion coefficients has been reported in olivine (Dohmen and Chakraborty 2007; Dohmen et al. 2007), FeO–MgO solid solutions (Yamazaki and Irifune 2003; Holzapfel et al. 2003), orthopyroxene (Dohmen et al. 2016), wadsleyite (Farber et al. 2000; Kubo et al. 2004; Holzapfel et al. 2009), and silicate melts (Zhang et al. 2010a).

Overall, if aforementioned influencing factors (T, P, f_{O_2}, C_{H_2O}, X_{Fe}) are simultaneously taken into account, the diffusion coefficient can be rewritten (Jaoul et al. 1995; Mackwell et al. 2005; Demouchy et al. 2007; Dohmen and Chakraborty 2007; Otsuka and Karato 2015):

$$D = D_0 (f_{O_2})^n (C_{H_2O})^r X^p \exp\left(-\frac{\Delta E + \alpha X + P\Delta V}{RT}\right) \quad (5)$$

where n, r, and p are constants, and α is a parameter related to the activation energy. Besides abovementioned issues, other affecting factors, including crystallographic orientation (anisotropy), isotope effect, stress and deformation, have been reviewed and discussed in detail by many researchers (Ganguly 2002; Mehrer 2007; Chakraborty 2008; Zhang 2010).

2.4 Experimental Measurement and Analysis Methods of Diffusion Coefficient

Diffusion experiments are frequently performed under high-pressure and high-temperature and controlled thermodynamic conditions (e.g., f_{O_2}, water content, silica activity), using

diffusion couple methods. The diffusion couples were made up of crystal↔crystal or crystal↔powder. Due to very limited laboratory time scales (usually less than one week) and accessible *P–T* conditions, the resultant diffusion profiles are very short. The diffusion rate of a given element is not only related to the nature of the element, but also depends on the properties of the diffusion medium. For example, Si is the slowest element in many of the mantle minerals, the diffusion distances are as short as several tens of nanometers even annealing at high pressure and high temperature for a longer time. Thus, such short diffusion profiles have necessitated the use of very precise analytical techniques.

Diffusion is quantified by measuring the concentration of the diffusing species at different distances from the release point after a given time has elapsed at a precise temperature. In general, two approaches, including direct profiling and bulk release/exchange, can be used to determine the diffusion coefficients in diffusion studies (Cherniak et al. 2010). Direct profiling methods, where the concentration of diffusant versus depth is determined, can be subdivided into methods involving step-scanning, with measurements made by stepping across a sample cut normal to the diffusion interface, and depth profiling, where analyses are performed parallel to the diffusion direction. Step-scanning may be used in cases where diffusion profiles are at least many tens of micrometers long, as it is limited by the beam spot size (typically ≥ 2 μm) of the analytical tool used and the minimum number of points necessary to define the diffusion profile. During the past forty years, the ion microprobe (Secondary Ion Mass Spectrometry, SIMS) instruments have made considerable technological advances with the development of Focused Ion Beam and nanoSIMS capabilities, which further improve spatial resolution. Accelerator-based ion beam techniques Rutherford backscattering spectrometry (RBS) have found increased application in diffusion studies of geological materials, with RBS used to measure diffusion of many medium to heavy elements in a variety of mineral phases, and Nuclear Reaction Analysis (NRA) and Elastic Recoil Detection (ERD) and Auger Electron Spectroscopy (AES) are also applied in measuring short diffusion distances; additional refinements of extant methods have enhanced their utility in studying geological samples. In addition, improvements in instrumentation and analytical protocols have also benefited the application of IR spectroscopy, synchrotron X-ray fluorescence (SRXRF), electron microprobe analysis (EPMA), and laser-ablation inductively coupled mass spectrometry (LA-ICP-MS) in measurement of diffusion profiles. On the other hand, indirect estimates (i.e., bulk release or exchange), mineral grains or crushed fragments of material are exposed to a reservoir containing a radiotracer or isotopically tagged tracer (typically an aqueous solution or gas source, depending on the diffusing species), with the degree of exchange determined using mass spectrometry (in the case of tracer isotopes) or counting of activity (in the case of radiotracers). However, such "bulk exchange" methods have several limitations (Cherniak et al. 2010), including assumptions are often made regarding diffusion models used to evaluate diffusivities, the difficulty in evaluating diffusional anisotropy, and of sorting out potential contributions from transport along extended defects or other diffusional "fast paths" from those of lattice diffusion when profiles are not directly measured. Once variation curve of the concentration of the diffusion element with the depth is available, one can calculate the diffusion coefficient by means of mathematical analysis to solve diffusion equation for a given boundary condition.

3 Available Results

3.1 Upper Mantle

3.1.1 Olivine

The first detailed study of Fe–Mg interdiffusion rates uptake in olivine was reported by Buening and Buseck (1973) at atmospheric pressure as a function of composition. Their data revealed a compositional dependence (diffusion rates increase with Fe content) and clear diffusion anisotropy (diffusion fastest along the [001] direction). Moreover, Buening and Buseck (1973) found a kink in the Arrhenius plot (Fig. 3) and argued that this kink could be due to either a change from intrinsic to extrinsic diffusion mechanism or due to a transition from lattice-controlled to grain-boundary-controlled diffusion introduced by the use of the fayalite powder in the diffusion couple experiments, whereas Chakraborty (1997) and Dohmen et al. (2007) pointed out that the concentration profiles obtained by Buening and Buseck (1973) were most likely affected by extreme convolution effects in their microprobe analyses. Misener (1974) carried out high-pressure Fe–Mg interdiffusion experiments in Fe-bearing olivine at pressure up to 3.5 GPa and between 1173 and 1373 K, resulting in an activation volume of 5.5 cm^3/mol. Similar experiments were later performed by Jaoul et al. (1995) at relatively low temperatures (873–1173 K) at 3–9 GPa and concluded that the activation volume is essentially zero. As Jaoul et al. (1995) could not yet vary the composition of their thin films and oxygen fugacity of their experiments in a controlled manner, it was not possible to analyze diffusion mechanisms in detail in their work. On the other hand, it is worth noting that, although they compared their experimental results to those of computer calculations, the fact that a dependence of experimentally observed diffusion rates on oxygen fugacity was postulated and the computer calculations were carried out on systems without Fe resulted in some inconsistency. Additional issue with Jaoul et al.'s data comes from the fayalite thin films deposited as the diffusion source in their experiments, because it is a difficult task to ensure the survival of the thin film at much more extreme chemical and mechanical conditions during high-pressure experiments. However, Jaoul et al. (1995) have not carried out any surface characterization with SEM and interference microscopy. This would be important because substantial re-crystallization of the film occurs leading to larger roughness and substantial convolution effects for any depth profiling method such as RBS (Dohmen et al. 2007). Consequently, the enormous scatter of diffusion data were reported by Jaoul et al. (1995) and the activation volume obtained in their work might be invalid. Chakraborty (1997) made Fe–Mg interdiffusion experiments at 980–1300 °C using synthetic Fe-free forsterite as one of the starting materials and found that the interdiffusion occurs in the transition metal extrinsic domain (TaMED), indicating that diffusion of cation vacancies is much faster than that of cations and vacancy concentrations in nominally Fe-free forsterite. Chakraborty et al. (1999) measured Fe–Mg interdiffusion in San Carlos olivine, at 1673 K between 9 and 12 GPa. An average activation volume of 0.35 cm^3/mol can be calculated from their data; however, this estimate is not reliable because of the limited number of data points. Farber et al. (2000) determined the pressure dependence of Fe–Mg interdiffusion in forsterite between 1 and 4GPa obtaining an activation volume of 5.4 ($\pm$4.0) cm^3/mol along the Ni–NiO buffer at 1473 K. and found very similar pressure dependence to that determined by Misener (1974). Their results, within errors, are in excellent agreement with other determinations reported by Misener (1974) (5.5 cm^3/mol) and Holzapfel et al. (2007)

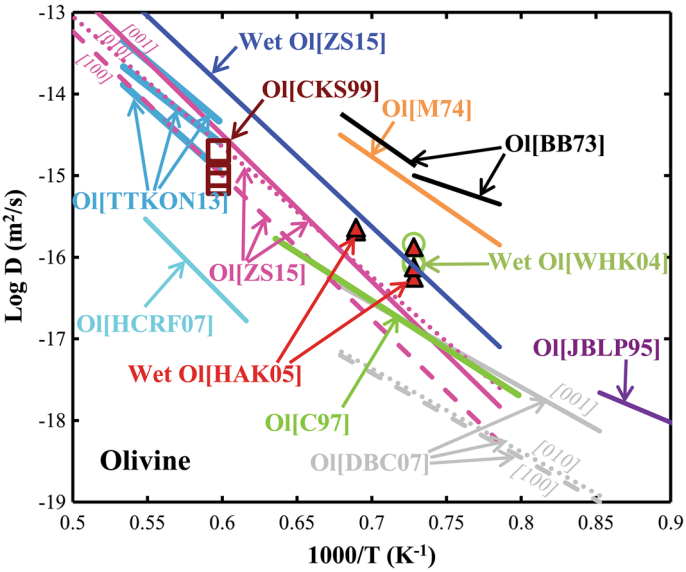

Fig. 3 Arrhenius plot summarizing experimental and calculated results for Fe–Mg interdiffusion in olivine. *Data source* M74 (Misener 1974), BB73 (Buening and Buseck 1973), JBLP95 (Jaoul et al. 1995), C97 (Chakraborty 1997), CKS99 (Chakraborty et al. 1999), WHK04 (Wang et al. 2004), HAK05 (Hier-Majumder et al. 2005), HCRF07 (Holzapfel et al. 2007), DBC07 (Dohmen et al. 2007), TTKON13 (Tachibana et al. 2013), ZS15 (Zhang and Shan 2015a). Arrhenius parameters (D_0 and ΔE) are summarized in Table 1

(5.3 cm^3/mol). Dohmen et al. (2007) measured Fe–Mg diffusion coefficients in olivines at atmospheric pressure as a function of composition, crystal orientation, oxygen fugacity and temperature (700–1200 °C) using thin films produced by pulsed laser deposition and RBS to analyze the concentration profiles. However, Fe–Mg diffusion in olivine is strongly dependent on the mole fraction of the Fe end-member, but weakly dependent/independent of f_{O_2}. Subsequently, Dohmen and Chakraborty (2007) have developed a quantitative point defect model to calculate Fe–Mg interdiffusion coefficients in olivine for modeling any natural process. The resulting master equations from Dohmen and Chakraborty (2007) can reproduce all of the 113 experimental data points within half an order of magnitude. Recently, Tachibana et al. (2013) investigated the interdiffusion coefficient of Fe–Mg in olivine at 1400–1600 °C at the atmospheric pressure with the oxygen fugacity of $10^{-3.5}$–10^{-2} Pa using diffusion couple method. Their results showed a clear anisotropy ($D_{Fe-Mg}[001] > D_{Fe-Mg}[010] > D_{Fe-Mg}[100]$), but little correlation with f_{O_2} and no significant compositional dependence of D_{Fe-Mg}. However, at higher temperature (>1400 °C), the increase in the activation energy of D_{Fe-Mg} has been interpreted as the result of the transition of diffusion mechanism from TaMED to the intrinsic domain at the atmospheric pressure (Tachibana et al. 2013). In a review of available Fe–Mg interdiffusion coefficients (D_{Fe-Mg}) in olivine in literatures, Chakraborty (2010) claimed that cation vacancies in olivine are controlled by the concentration of ferric iron determined by ambient temperature and oxygen fugacity conditions in the temperature range for magmatic processes and thus that the Fe–Mg interdiffusion in olivine occurs by TaMED mechanism (Chakraborty 1997; Dohmen et al. 2007; Dohmen and Chakraborty 2007). For a detailed discussion, calculation, and experimental demonstration of diffusion by TaMED, pure extrinsic

diffusion (PED) and intrinsic diffusion mechanisms in olivine, the reader can refer to the papers by Dohmen et al. (2007) and Dohmen and Chakraborty (2007) and Chakraborty (2008).

On the other hand, it is well known that water, even a small amount, may has significant influence on some of the key physical and chemical properties in minerals (e.g., melting relationship, electrical conductivity, rheological properties and diffusivity). To better understand the effect of water on diffusion, Wang et al. (2004) performed Fe–Mg interdiffusion experiments in olivine under water-saturated conditions at 1373 K and 300 MPa, indicating that the interdiffusion of Fe–Mg in olivine under hydrous conditions is about one order of magnitude greater than under anhydrous conditions. Also, this effect has been studied by Hier-Majumder et al. (2005). Their results showed that the interdiffusivity increases by a factor of 50 at 1373 K and 5 GPa for an increase in water content from 100 to 8100 ppm H/Si. The activation volume of 16 cm^3/mol obtained by Hier-Majumder et al. (2005) under wet conditions is almost three times larger than that under dry conditions (see Table 1), this observation implies that diffusion under hydrous conditions may occur by a different mechanism (Chakraborty 2010). However, no systematic experimental data was reported on water effect on Fe–Mg interdiffusion in olivine so far. Thus, this issue remains unsolved. In addition, the interdiffusivities of Fe–Mg in single crystal and polycrystal olivine have been calculated in the light of a thermodynamic approach (Zhang and Shan 2015a), the refined data agree well with the experimentally reported ones (Fig. 3).

3.1.2 Pyroxenes

Pyroxenes are major mineral phases at depth (in the lower crust and upper mantle) in both the earth and extraterrestrial bodies. Dimanov and Sautter (2000) investigated (Fe, Mn)–Mg interdiffusion in single crystals of natural diopside (X_{Fe} 0.03) at ambient pressure, high temperatures (900–1240 °C) and low-oxygen fugacity by both RBS and SIMS. Afterward, Dimanov and Wiedenbeck (2006) extended the study of Dimanov and Sautter (2000), focusing on the effects of oxygen fugacity. As shown in Fig. 4, it can be seen that the experimental results of Dimanov and Sautter (2000) and Dimanov and Wiedenbeck (2006) are in reasonably good agreement both in terms of magnitude of diffusivities and activation energy after pO_2 corrections are made to the former dataset. Both datasets still differ by about half an order of magnitude, but this moderate discrepancy may result from the Early Partial Melting (EPM) within the host diopside because EPM can significantly affect the point defect chemistry of the material and thus influences all f_{O_2}-dependent transport properties including ionic diffusion. Previous study (Jaoul and Reterron 1994) has shown that EPM occurrence depends essentially on oxygen fugacity, temperature and initial non-stoichiometry. In fact, EPM was clearly observed above 1150 °C in the experiment of Dimanov and Wiedenbeck (2006). Recently, Müller et al. (2013) reported Fe–Mg interdiffusion rates in natural diopside crystals ($X_{Di} = 0.93$) along the c axis in the geologically relevant temperature range of 800–1200 °C from experiments carried out at atmospheric pressure under controlled oxygen fugacity conditions. Their data demonstrated that diffusion in clinopyroxene may be the rate-limiting process for the freezing of many geothermometers, and compositional zoning in clinopyroxene may preserve records of a higher temperature segment of the thermal history of a rock. In addition, no strong dependence of D_{Fe-Mg} on composition of clinopyroxene or oxygen fugacity could be detected within the resolution of the study by Müller et al. (2013). This observation suggested that higher Al concentrations of the pyroxene would have produced charge compensation Fe^{3+} that overwhelmed the concentration of vacancies generated by

oxidation of Fe^{2+} in the clinopyroxene structure, variation in f_{O_2} and the resulting change in concentration of Fe^{3+} does not have any significant influence on vacancy concentrations and hence on diffusion rates.

So far as we know, direct experimental measurements of D_{Fe-Mg} in orthopyroxene are very difficult because of very slow rate of Fe–Mg interdiffusion. Ganguly and Tazzoli (1994) made the first indirect estimates of Fe–Mg interdiffusion rates in orthopyroxenes on the basis of the rates of order–disorder kinetics of Fe and Mg fractionation between the M1 and M2 sites in orthopyroxene that were measured experimentally in the temperature range of 500–800 °C at an f_{O_2} at, or close to, IW. Consequently, the predicted D_{Fe-Mg} in orthopyroxenes from a theoretical relationship between diffusion and order–disorder properties developed by Ganguly and Tazzoli (1994) are comparable to the available experimental data (Fig. 4). Dohmen et al. (2016) directly measured Fe–Mg interdiffusion coefficients parallel to the three main crystallographic axes between 870 and 1100 °C in two natural orthopyroxene single crystals under atmospheric pressure and between controlled oxygen fugacity of 10^{-11} and 10^{-7} Pa. They found that the anisotropy of diffusion D_{Fe-Mg} follows the sequence $D_{Fe-Mg}[001] \approx D_{Fe-Mg}[010] \approx 3.5D_{Fe-Mg}[100]$, and diffusion in natural orthopyroxene becomes insensitive to f_{O_2} when f_{O_2} around or lower the IW buffer. This investigation could be related to a transition in the diffusion mechanism from TaMED to PED.

3.1.3 Garnet

Garnet is an important rock-forming mineral of various magmatic, metamorphic and metasomatic rocks. Because of the flexibility provided by many possible end-member compositions, garnets are formed in many different lithologies and at various *P–T* conditions of the Earth's crust and mantle. The composition of garnet is very sensitive to these parameters and thus variations often lead to the formation of zoned crystals. In this study, only diffusion data for Fe–Mg rich, Mn-poor garnets are discussed. Elphick et al. (1985) reported the first credible results on divalent cation diffusion kinetics in garnet at high *P–T* conditions (30–40 kbar, 1300–1500 °C), using diffusion couples made from natural garnet crystals. Their data indicated that the multicomponent diffusion kinetics in garnet strongly depend on Mg/Mn ratio. Consequently, Fe–Mg interdiffusion is one order of magnitude slower than Fe–Mn interdiffusion in garnet. Ganguly et al. (1998) carried out diffusion couple experiments consisting of natural pyrope and almandine garnets at 2.2–4.0 GPa, 1330–1673 K in a piston-cylinder apparatus to determine the self-diffusion coefficients of the divalent cations Fe, Mg, Mn and Ca. It is found that the self-diffusion of Fe and Mn is significantly enhanced with the increase in Mn/Mg ratio; the enhancement effect on D_{Mg} is relatively small. Moreover, Ganguly et al. (1998) developed and tested a numerical method to deconvolve the tracer diffusion coefficients retrieved from modeling multicomponent diffusion profiles in the pyrope–almandine couples. Freer and Edwards (1999) performed Ca–(Fe, Mg) interdiffusion experiments between grossular and almandine single crystals, and measured the activation volume at 1273 K between 1.5 and 3.2 GPa. They found a very high value (11.2 cm^3/mol) for the activation volume, for which they could not offer a plausible explanation. Borinski et al. (2012) carried out diffusion couple experiments (25–35 kbar and 1260–1400 °C) to determine Fe–Mg interdiffusion coefficients in garnet in a piston-cylinder apparatus using natural pyrope and almandine crystals. Also, Borinski et al. (2012) have developed and tested a numerical method to calculate best-fit diffusion coefficients from experimentally induced concentration profiles. As a consequence, diffusion coefficients D_{Fe-Mg} retrieved using the two kinds of models do

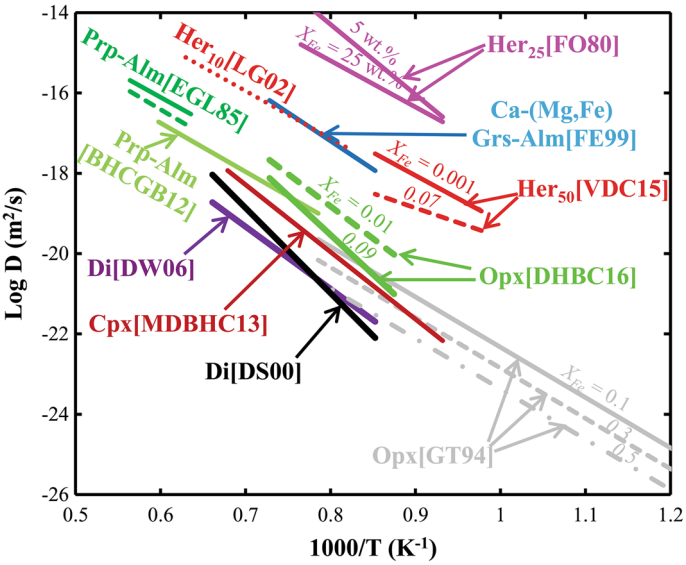

Fig. 4 Arrhenius plot summarizing experimental results for Fe–Mg interdiffusion in pyroxene, garnet and spinel. *Data source* Opx-GT94 (Ganguly and Tazzoli 1994), Opx–DHBC16 (Dohmen et al. 2016), Cpx–MDBHC13 (Müller et al. 2013), Di–DS00 (Dimanov and Sautter 2000), Di–DW06 (Dimanov and Wiedenbeck 2006), Prp–Alm–EGL85 (Elphick et al. 1985), Prp–Alm–BHCGB12 (Borinski et al. 2012), Grs–Alm–FE99 (Freer and Edwards 1999), Her_{10}–LG02 (Liermann and Ganguly 2002), Her_{25}–FO80 (Freer and O'Reilly 1980), Her_{50}–VDC15 (Vogt et al. 2015). Arrhenius parameters (D_0 and ΔE) are summarized in Table 2

not differ from those experimentally reported data for most natural garnet compositions. As shown in Fig. 4, the diffusivities retrieved by Freer and Edwards (1999) are higher than for other experimental data (Elphick et al. 1985; Borinski et al. 2012).

3.1.4 Spinel

Spinel ($Fe_xMg_{1-x}Al_2O_4$) is one of the major minerals in Earth's uppermost mantle, a common mineral in a wide range of metamorphic and ultramafic rocks, and an important mineral inclusion found in chondritic meteorites of the early Solar System, and it has also been found in lunar rocks. Spinel has cubic symmetry, and diffusion is therefore isotropic. Spinel also contains octahedral interstitial sites, and two different types of tetrahedral interstitial sites (Van Orman and Crispin 2010).

Freer and O'Reilly (1980) were the first to determine the activation energy and the Fe–Mg interdiffusion coefficient, D_{Fe-Mg} in aluminous spinel as a function of temperature (800–1034 °C) and composition ($FeAl_2O_4$–$MgAl_2O_4$) using diffusion couples composed of synthetic pellets. Their data reveal a strong compositional dependency where D_{Fe-Mg} increases with decreasing Fe^{2+} content in spinel. Liermann and Ganguly (2002) performed the diffusion kinetics of Fe^{2+} and Mg in spinel ($Mg_{0.99}Fe_{0.01}Al_{1.997}Cr_{0.003}O_4$) using diffusion couples at 2 GPa, 950–1325 °C and at 3 GPa and 1125 °C. Interdiffusion coefficients determined by Freer and O'Reilly (1980) are about two orders of magnitude higher than those determined by Liermann and Ganguly (2002) (Fig. 4). Also, Freer and O'Reilly (1980) found complicated diffusion profiles that appeared to indicate strong

compositional dependence of the interdiffusion coefficient, while Liermann and Ganguly (2002) found simple error function diffusion profiles that indicated a negligible influence of iron concentration. The discrepancies between these two studies might be related to differences in oxygen fugacity. More recently, Vogt et al. (2015) measured Fe–Mg interdiffusion rates ($D_{\mathrm{Fe–Mg}}$) in synthetic Mg–Al spinel and a natural (Mg, Fe) aluminous spinel using diffusion couples made of single-crystal spinel and thin films of hercynitic composition (X_{Fe} 0.5) at atmospheric pressure over a range of different oxygen fugacities and temperatures (750–900 °C). Their results showed that $D_{\mathrm{Fe–Mg}}$ in Mg-spinel is independent of oxygen fugacity, whereas it depends strongly and nonlinearly on oxygen fugacity for the natural spinel. This observation indicates that the mechanisms of diffusion are different in the two kinds of spinel (Fe-bearing vs. Fe-free). The nonlinear dependence on oxygen fugacity indicates that diffusion occurs by an interstitial mechanism at low-oxygen fugacities and by a vacancy mechanism at high-oxygen fugacities in natural, Fe-bearing spinel. As illustrated in Fig. 4, comparison of the Fe–Mg interdiffusion rates determined by Vogt et al. (2015) with those of Liermann and Ganguly (2002) implies a good agreement between Vogt et al.'s and Liermann and Ganguly's results in Mg–Al spinel. Moreover, as seen from Fig. 4, the diffusivities reported by Freer and O'Reilly (1980) (for a spinel composition of FeO = 25 wt% and FeO = 5 wt%) are three to four orders of magnitude higher than those obtained by Vogt et al. (2015) and Liermann and Ganguly (2002). Nevertheless, Vogt et al. (2015) demonstrated that, when the diffusion mechanism and the nonlinear dependence of $D_{\mathrm{Fe–Mg}}$ on f_{O_2} are considered, all experimental datasets (Freer and O'Reilly 1980; Liermann and Ganguly 2002; Vogt et al. 2015) can be completely reproduced by a point defect thermodynamic model and are in fact consistent with each other (see Fig. 10 of Vogt et al. 2015).

3.2 Transition Zone

3.2.1 Wadsleyite and Ringwoodite

Wadsleyite and ringwoodite (named β-spinel and γ-spinel) are high-pressure polymorphs of olivine that are found in shocked meteorites and are thought to be the minerals that replace olivine with increasing the depth in the transition zone (ca. 410–660 km depth) of the Earth's mantle. Wadsleyite has an orthorhombic structure, whereas ringwoodite is cubic. Diffusion rates in wadsleyite and ringwoodite are very difficult to measure because crystals large enough in size to measure diffusion coefficients are difficult to obtain. The other difficulties related to high-pressure experiments include the issues of controlling oxygen fugacity and water contents, and the limited stability ranges of these phases. As a result, it is impossible to carry out experiments over large ranges of temperatures and pressures to constrain parameters such as activation volume and activation energy well. Diffusion coefficients of wadsleyite and ringwoodite are known from measurements in coarse polycrystals and in rare single crystals.

Chakraborty et al. (1999) first reported the Fe–Mg interdiffusion rates in wadsleyite using single crystal ↔ polycrystal diffusion couples at 15 GPa and 1373–1473 K. Subsequently, three other studies have measured Fe–Mg diffusion rates in wadsleyite (Farber et al. 2000; Kubo et al. 2004; Holzapfel et al. 2009) and these results have been analyzed together and discussed by Holzapfel et al. (2009). Combining the data from Farber et al. (2000) and Kubo et al. (2004), Holzapfel et al. (2009) obtained the following global relationship for calculating Fe–Mg diffusion coefficients in wadsleyite as a function of

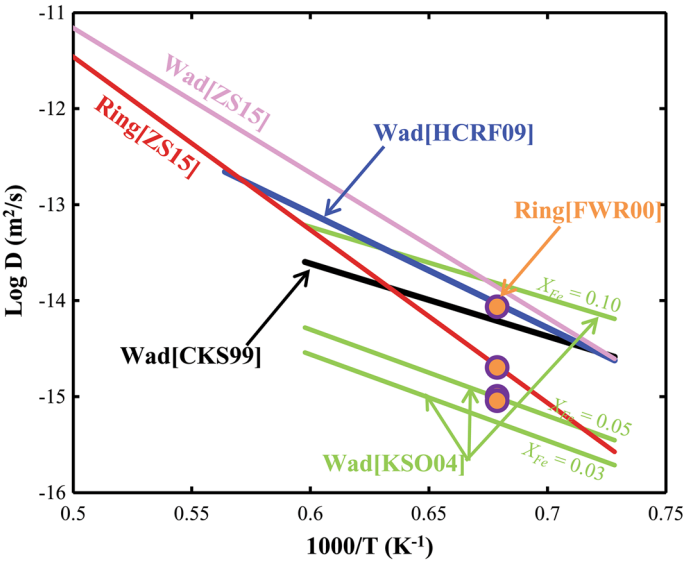

Fig. 5 Arrhenius plot summarizing experimental and calculated results for Fe–Mg interdiffusion in wadsleyite and ringwoodite *Data source* CKS99 (Chakraborty et al. 1999), KSO04 (Kubo et al. 2004), HCRF09 (Holzapfel et al. 2009), FWR00 (Farber et al. 2000), ZS15 (Zhang and Shan 2015a). Arrhenius parameters (D_0 and ΔE) are summarized in Table 3

temperature, pressure and composition under dry (less than several tens of ppm H_2O) conditions and with f_{O_2} lying along the NNO equilibrium:

$$D(\mathrm{m}^2/\mathrm{s}) = 1.24 \times 10^{-6} \exp\left[11.8(0.86 - X_{\mathrm{Mg}})\right] \exp\left(\frac{-[229000 + (P - 15) \times 13.9 \times 10^3]\mathrm{J/mol}}{RT}\right)$$

where X_{Mg} is the mole fraction of Mg in wadsleyite, T is the absolute temperature in Kelvins, and P is the pressure in GPa. However, a very large activation volume 13.9 cm^3/mol suggests that the effect of pressure on Fe–Mg interdiffusion in wadsleyite is strong. It must be pointed out that this equation is valid for oxygen fugacity at the NNO buffer and for dry conditions. Up to date, only Farber et al. (2000) measured Fe–Mg interdiffusion coefficients in ringwoodite at 1473 K and 10–14 GPa. They obtained an activation volume 6.1 cm^3/mol, but failed to constrain the activation energy for Fe–Mg diffusion in ringwoodite. All Fe–Mg interdiffusion data obtained in wadsleyite and ringwoodite are summarized in Table 3, and also compared with those results from the thermodynamic calculations by Zhang and Shan (2015a) in Fig. 5.

3.3 Lower Mantle

3.3.1 Bridgmanite

Silicate bridgmanite (Mg, Fe)SiO_3 is believed to be the dominant phase in the Earth's lower mantle, possibly in excess of 80% of the total volume (e.g., Ringwood 1975). Hence, an understanding of the diffusion properties of bridgmanite is therefore necessary for constraining processes such as mantle convection, homogenization of chemical

heterogeneities, interaction with metal during core formation, and the extent of reactions occurring at the core-mantle boundary. Only few diffusion studies exist for high-pressure phases, such as bridgmanite. The reason for this lack of data is the difficulty of maintaining high pressure and temperature conditions to stabilize the high-pressure phases for such a long time that diffusion profiles can be measured. Holzapfel et al. (2005) measured Fe–Mg interdiffusion in (Mg, Fe)SiO_3 bridgmanite at pressures from 22–26 GPa and temperatures between 1973–2273 K. High-pressure interdiffusion experiments were conducted on polycrystalline bridgmanite diffusion couples, each consisting of a disk of initially Fe-free $MgSiO_3$ bridgmanite in contact with a second disk of Fe-bearing bridgmanite in which $X_{Fe} = 0.02$–0.11, employing a multi-anvil apparatus. The diffusion couples were contained either Ni or MgO capsules; oxygen fugacity was estimated to be about 3 log-units below the iron–wüstite buffer (IW-3) for MgO capsules and 3 log-units above the IW buffer (IW + 3) for Ni capsules. In their experiments, no compositional dependence on Fe–Mg diffusion was detected, and nor any dependence on orientation. They found that Fe–Mg interdiffusion in bridgmanite is as slow as Si self-diffusion and is orders of magnitude slower than Fe–Mg diffusion in other mantle minerals. Holzapfel et al. (2005) derived an Arrhenius relation from the data for diffusion at 24 GPa assuming that the pre-exponential factor depends on f_{O_2} while the activation energy for diffusion is independent of f_{O_2}, obtaining a pre-exponential factor of 4.0 ($\pm$0.7) $\times$ 10^{-9} m^2/s for reducing conditions (IW-3) and 7.9 ($\pm$1.4) $\times$ 10^{-8} m^2/s for oxidizing conditions (IW + 3), and an activation energy of 414 ($\pm$62) kJ/mol (Table 4). However, Holzapfel et al. (2005) were unable to achieve a large enough pressure range in their experiments to establish an activation volume for Fe–Mg diffusion. Xu et al. (2011) for the first time measured Si and Mg self-diffusion coefficients in single crystals of bridgmanite under lower mantle conditions. Their results showed that no anisotropy in the diffusion of either Si or Mg could be resolved and Mg has very similar diffusivity to Si in bridgmanite. Recently, Zhang and Shan (2015a) predicted the Fe–Mg interdiffusion coefficients in bridgmanite as a function of temperature and pressure using a thermodynamic model that interconnected point defect parameters with the bulk properties. As depicted in Fig. 6a, theoretically calculated results are consistent with the experimental ones roughly between IW-3 and IW + 3, whereas the activation energy of 646 kJ/mol is higher than that of 414 kJ/mol reported by Holzapfel et al. (2005).

3.3.2 Ferropericliase

Ferropericlase (Mg, Fe)O is the second most abundant phase in the Earth's lower mantle next to silicate bridgmanite. Previous studies have shown that ferropericlase (Mg, Fe)O has noticeably higher atomic diffusivity (Holzapfel et al. 2003; Yamazaki and Irifune 2003), low viscosity (Yamazaki and Karato 2001), and higher electrical conductivity (Dobson et al. 1997; Yoshino et al. 2011) than bridgmanite. Thus, it is possible that (Mg, Fe)O has a strong influence in defining bulk transport properties in the lower mantle especially when it forms an interconnected network, even though interconnected locally. Several groups (Yamazaki and Irifune 2003; Holzapfel et al. 2003; Mackwell et al. 2005) have examined the effects of temperature, pressure and oxygen fugacity on Fe–Mg interdiffusion in ferropericlase (Mg, Fe)O. Under dry conditions, Fe–Mg interdiffusion rates increase with increasing iron content and oxygen fugacity, but decrease with increasing pressure by 2.5 orders of magnitude from one atmosphere to 23 GPa (Mackwell et al. 2005). Subsequently, Demouchy et al. (2007) found that Fe–Mg interdiffusion is enhanced by the presence of hydrogen (protons) in (Mg, Fe)O even at relatively low pressure of 300 MPa. They attributed the enhancement of interdiffusion rate to the increased concentration of metal

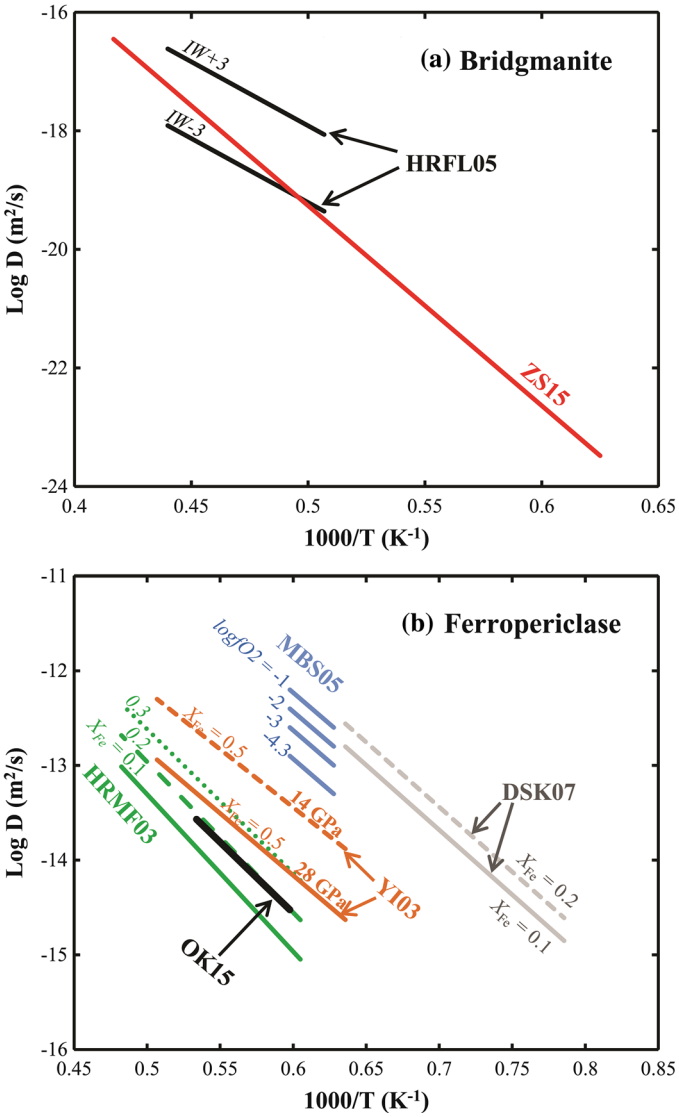

Fig. 6 Arrhenius plot summarizing experimental and calculated results for Fe–Mg interdiffusion in **a** bridgmanite and **b** ferropericlase. *Data source* HRFL05 (Holzapfel et al. 2005), YI03 (Yamazaki and Irifune 2003), HRMF03 (Holzapfel et al. 2003), MBS05 (Mackwell et al. 2005), DSK07 (Demouchy et al. 2007), OK15 (Otsuka and Karato 2015), ZS15 (Zhang and Shan 2015a). Arrhenius parameters (D_0 and ΔE) are summarized in Table 4

vacancies resulting from the incorporation of hydrogen. Otsuka and Karato (2015) systematically investigated the influence of Fe^{3+} and H^+ on Fe–Mg interdiffusion in (Mg, Fe)O at 1673–1873 K and 5–24 GPa under the anhydrous and hydrous conditions using the diffusion couple technique. Their results showed that the dominant defect responsible for diffusion is same under both anhydrous and hydrous conditions, suggesting that H^+ enhances Fe–Mg interdiffusivity by promoting the mobility of vacancies at the M-site. The

influence of Fe^{3+} likely dominates at temperatures expected for the normal lower mantle conditions ($T > 1900$ K), while the influence of both Fe^{3+} and H^{+} is important at lower temperature environments such as near the subduction zone. All abovementioned data are summarized in Fig. 6b and Table 4 along with the reported activation volume.

3.4 Comparison with Fe—Mg Interdiffusion in Mantle Minerals

In Fig. 7a, we compare the experimental D_{Fe-Mg} with the theoretical estimates in major mantle minerals. It is obvious that diffusion of Fe–Mg in bridgmanite is the slowest-diffusing case (Holzapfel et al. 2005). Diffusion rates of Fe–Mg in orthopyroxene (Ganguly and Tazzoli 1994; Dohmen et al. 2016) are similar to the rates of diffusion in clinopyroxenes (Müller et al. 2013), diopside (Dimanov and Sautter 2000; Dimanov and Wiedenbeck 2006) and garnet (Elphick et al. 1985; Freer and Edwards 1999; Borinski et al. 2012). Fe–Mg interdiffusivities in dry olivine (Jaoul et al., 1995; Chakraborty 1997; Chakraborty et al. 1999; Dohmen et al. 2007; Holzapfel et al. 2007; Tachibana et al. 2013) are comparable to those observed in spinel (Liermann and Ganguly 2002; Vogt et al. 2015), while slower than the diffusion rates in hydrous olivine (Wang et al. 2004; Hier-Majumder et al. 2005; Zhang and Shan 2015a) and olivine high-pressure polymorphs (Chakraborty et al. 1999; Farber et al. 2000; Kubo et al. 2004; Holzapfel et al. 2009). The rates of Fe–Mg interdiffusion in spinel reported by Freer and O'Reilly (1980) are the fastest ones among the existing data in mantle minerals, which are compatible with the experimental determinations in ferropericlase (Mackwell et al. 2005; Demouchy et al. 2007) and olivine high-pressure polymorphs, i.e., wadsleyite (Chakraborty et al. 1999; Holzapfel et al. 2009; Zhang and Shan 2015a) and ringwoodite (Zhang and Shan 2015a).

Besides the temperature dependence, pressure can also modify diffusion coefficients substantially. In order to manifest this effect, as shown in Fig. 7b, Fe–Mg interdiffusion coefficients in olivine, garnet and spinel were calculated as a function of pressure at a constant temperature by employing the experimentally determined diffusion parameters (D_0, ΔE and ΔV) summarized in Tables 1 and 2. However, the pressure dependence of Fe–Mg interdiffusion for olivine high-pressure polymorphs (wadsleyite and ringwoodite) and bridgmanite have been calculated previously (Zhang and Shan 2015a). In addition, although the rates of Fe–Mg interdiffusion in minerals could be significantly enhanced by water (Wang et al. 2004; Hier-Majumder et al. 2005; Demouchy et al. 2007; Otsuka and Karato 2015), unfortunately, no systematic and quantitative experimental results on this issue were reported for various mantle minerals so far. Therefore, it is unlikely to quantitatively compare the effect of water on Fe–Mg interdiffusivity in each mineral.

3.5 Observation of Compensation Law for Fe—Mg Interdiffusion

As discussed above, we consider Fe–Mg interdiffusion data from all published experimental measurements on single crystals and polycrystals of mantle minerals performed under nominally dry and hydrous conditions, and try to figure out some inherent relationships among these data. One effective way is to examine whether all of diffusion datasets obey the compensation law or not (Brady and Cherniak 2010; Jones 2014). The compensation law, termed the "isokinetic effect" or Meyer–Neldel rule (MNR), refers to a positive linear relationship between the activation energy (E) and the natural logarithm of the pre-exponential factor ($\ln D_0$):

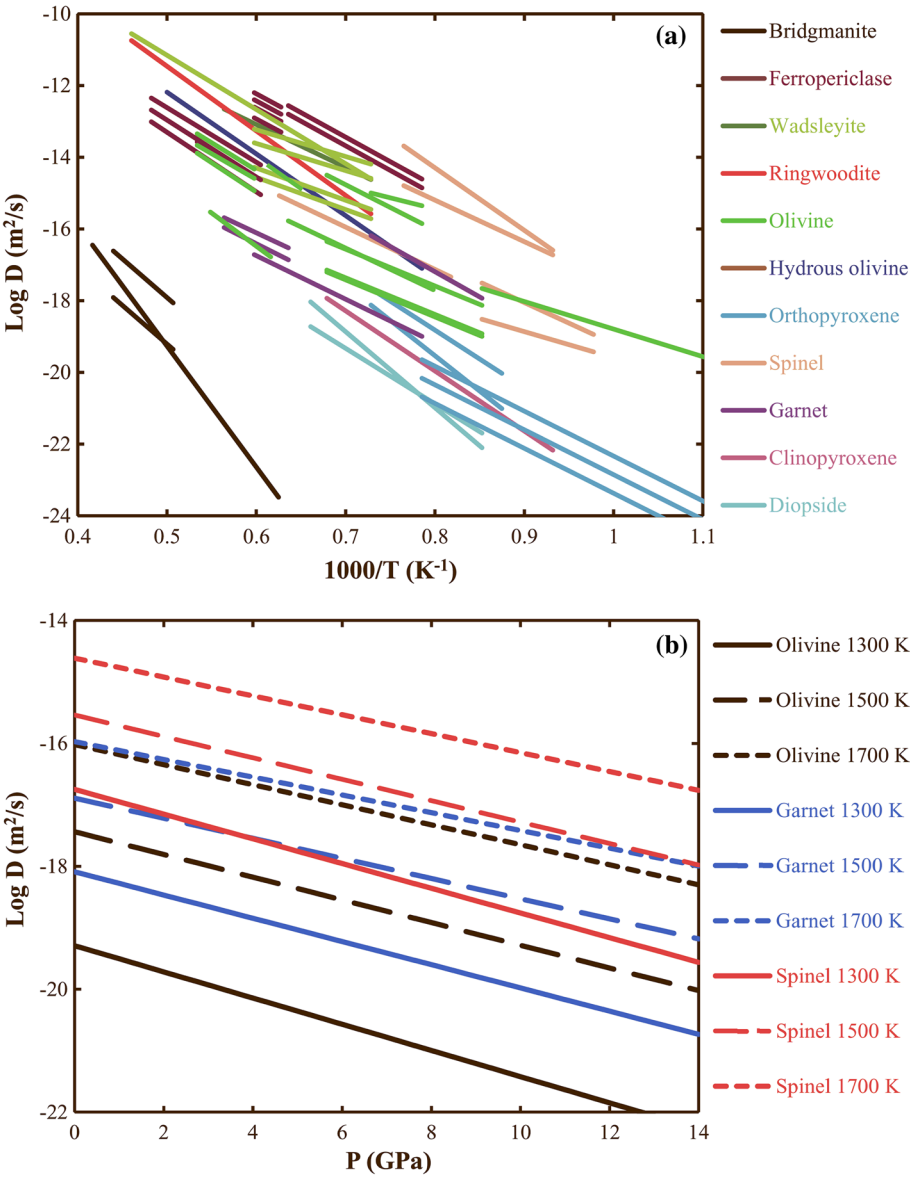

Fig. 7 **a** Arrhenius lines for Fe–Mg interdiffusion as reported for all mantle minerals in the database. **b** A comparison of the calculated Fe–Mg interdiffusivity in olivine (Holzapfel et al. 2007), garnet (Elphick et al. 1985) and spinel (Liermann and Ganguly 2002) as a function of pressure at constant temperature

$$\ln D_0 = \alpha + \beta E \tag{6}$$

where α and β are constants. If Eqs. (1) and (6) are combined in light of the MNR, then we can get $T_C = (\beta R)^{-1}$, here T_C is called the "characteristic temperature". This implies that if

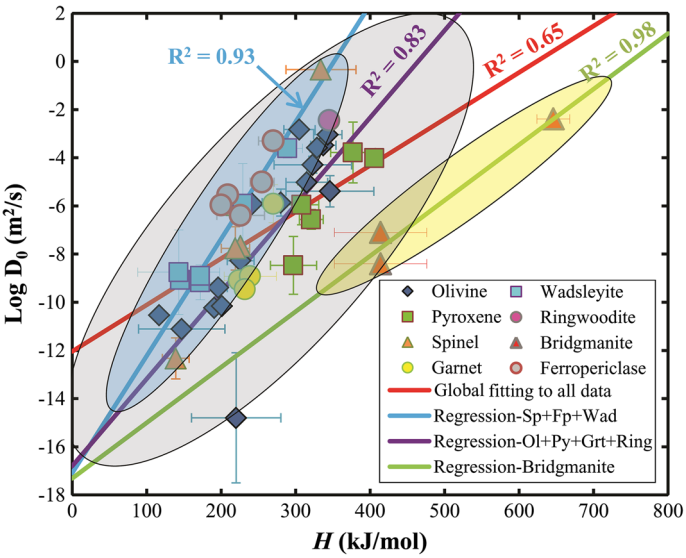

Fig. 8 Compensation plot of the experimentally determined pre-exponential factor ($\log D_0$) versus activation energy (E) for Fe–Mg interdiffusion in mantle minerals. Least-squares regressions to all data, group 1 (Sp + Fp + Wad), group 2 (Ol + Py + Grt + Ring) and group 3 (bridgmanite) subsets shown. *Red solid line* denotes the best fit to all of experimental data. The *regression line*: $\log D_0$ (m^2/s) = 0.01931 (0.0035)E (kJ/mol) −12.0445(1.0030) ($R^2 \approx 0.65$)

MNR exists in the substance, the diffusion tends to converge to a constant $D_C = \exp(\alpha)$ at T_C.

In the geosciences, to date, numerous studies have shown that the MNR is upheld not only for many diffusing species in individual minerals (Hart 1981), but also for a single diffusing species in a wide variety of minerals (Béjina and Jaoul 1997; Zheng and Fu 1998; Zhao and Zheng 2007; Zhang et al. 2010b, 2011; Brady and Cherniak 2010; Jones 2014; Zhang and Shan 2015b). Such an empirical law may provide an alternative possible insight coming from consideration of the experimental results of Fe–Mg interdiffusion in mantle minerals. In the present study, the experimental determined values of $\log_{10}(D_0)$ and E for all minerals, particularly those of interest to Earth's crustal, upper mantle, transition zone and lower mantle minerals for which the most extensive experimental or theoretical observations exist (see Tables 1, 2, 3, 4) including 45 diffusion measurements on 8 kinds of minerals, are plotted in Fig. 8, together with best-fitting robust linear regressions to all of the data and various subsets as well value of R^2. Note that there are three compensation lines corresponding to three subsets data, group 1 (Spinel + Ferropericlase + Wadsleyite, light blue field in Fig. 8), group 2 (Olivine + Pyroxene + Garnet + Ringwoodite, light gray field in Fig. 8), group 3 (bridgmanite, dark yellow field in Fig. 8), showing better correlation ($R^2 > 0.83$) than that ($R^2 > 0.65$) of the global fitting to all of data. Nonetheless, the data to create the compensation diagram are arbitrarily selected. For example, the compensation line for bridgmanite includes only three data points. However, one must be cautious when applying such compensation law to predict diffusion data.

Brady and Cherniak (2010) compiled the published experimental diffusion data and attempted to create the MNR compensation diagrams. Their investigations showed that different groups of elements yield systematically different compensation relations, which

strongly depends on the charge of cations. Especially, the Fe–Mg interdiffusion compensation line constructed by Brady and Cherniak (2010) has an R^2 value of only 0.36. Recently, Jones (2014) found that hydrogen diffusion in crustal and mantle minerals obeys different MNR. Indeed, similar phenomena have been observed for Si self-diffusion in mantle minerals (Zhang and Shan 2015b). In the case of Fe–Mg interdiffusion, experimentally reported interdiffusion data are not available in sufficient numbers to give meaningful compensation diagrams. It is worth noting that many factors make interdiffusion more complex than self-diffusion or tracer diffusion, typically including a strong dependence on composition that may include a thermodynamic factor (Ganguly 2002) and be especially sensitive to f_{O_2} or f_{H_2O}. In addition, different compensation trends revealed in this study may also reflect the complexity of substitutional processes and different diffusion mechanisms for Fe–Mg interdiffusion in various minerals (Brady and Cherniak 2010).

Moreover, on the basis of the observed MNR, a thermodynamic model (so-called the cBΩ model) has been successfully applied to predict diffusion coefficients of various elements in silicate minerals (Zhang et al. 2010b, 2011; Zhang 2012; Zhang and Shan 2015b). Although several assumptions and simplification have been made in the cBΩ model, the calculated diffusion parameters are reasonably comparable to the results reported experimentally when the uncertainties are considered, including Fe–Mg interdiffusion in $(Fe, Mg)_2SiO_4$ polymorphs and bridgmanite (Zhang and Shan 2015a).

4 Geoscience Applications

Experimental quantification of diffusion in the Earth's materials may in some cases enhance our understanding of a particular process or in others simply allow us to better constrain the temporal and/or spatial range over which a particular process may be important. Brady and Cherniak (2010) have demonstrated that the MNR is a powerful tool for calibrating and verifying determinations of the Arrhenius pre-exponent term and activation energy term fitting experimental data. Based on the foregoing discussions, the relative magnitude of Fe–Mg interdiffusion coefficients that can be used for modeling processes in natural systems (Fig. 7). Many workers have provided lots of examples of general applications of diffusion data in a number of minerals (e.g., Ganguly 2002; Watson and Baxter 2007; Brady and Cherniak 2010; Chakraborty 2008, 2010; Mueller et al. 2010). In view of published experimental datasets on Fe–Mg interdiffusion in mantle minerals, here I will merely outline some areas of application:

- Establish the diffusion-depth profile in the deep Earth (Yamazaki and Irifune 2003; Holzapfel et al. 2007; Watson and Baxter 2007) and evaluate diffusive equilibration time scales in the lower mantle (Holzapfel et al. 2005).
- Evaluate the closure temperature of geothermometry, geospeedometry, and time scales of geological and planetary processes (Jaoul et al. 1995; Chakraborty 1997, 2008; Ganguly 2002; Borinski et al. 2012; Müller et al. 2013; Dohmen et al. 2016).
- Understand the electrical conductivity profile of the Earth's mantle (Farber et al. 2000; Hier-Majumder et al. 2005; Otsuka and Karato 2015).
- Evaluate diffusive fractionation of isotopes in mantle rocks, meteorites and metamorphic rocks (Liermann and Ganguly 2002; Watson and Baxter 2007).
- Understand homogenization of mantle heterogeneities (chemical mixing) and mineral transformations (Chakraborty et al. 1999; Farber et al. 2000; Holzapfel et al. 2009).

- Understand the kinetics of order–disorder and intracrystalline exchange reaction (Ganguly and Tazzoli 1994).
- Understand the redox state of the mantle (Dohmen et al. 2007; Dohmen and Chakraborty 2007).
- Understand the rheological properties of the lower mantle (Demouchy et al. 2007).

5 Concluding Remarks and Perspectives

In this study, I provide a comprehensive review of the current state of Fe–Mg interdiffusion in major mantle minerals. Recently, new advances in the experimental technologies (e.g., Béjina et al. 2003; Yamazaki and Irifune 2003; Holzapfel et al. 2005; Brady and Cherniak 2010) and computational approaches (e.g., Béjina et al. 2009; Ammann et al. 2010; Ito and Toriumi 2010) have been available to explore diffusion in the deep Earth (i.e., $P > 25$ GPa), and to help us model processes in natural systems occurring on a variety of timescales. One important general conclusion is that the diffusion coefficients of any elements depend on minerals as well as pressure, temperature, composition, and other chemical parameters (such as oxygen fugacity and water fugacity). Consequently, diffusion coefficients likely change with physical and chemical conditions. Results obtained under limited conditions should not be applied to other conditions without appropriate corrections. The data obtained in the experimental determination of diffusion coefficients may play an important role in many areas of geochemistry and geophysics.

Major progress has been made on Fe–Mg interdiffusion in mantle minerals in the past several decades, together with the improvements on high-pressure experimental techniques in multi-anvil apparatus and the development of new analytical tools. However, some significant points still remain challenging, and a number of issues need to be explored in more detail:

1. Vacancies, dislocations, and other crystal defects may have profound effects on diffusion rates. Therefore, it is essential that the mineral being studied is well-characterized. If the diffusion medium (mineral, liquid, or glass) contains variable valence element like Fe, the oxygen fugacity of the equilibrium system should be controlled precisely because of its influence on the defect concentration. Therefore, defect chemistry in turn affects a number of physico-chemical properties of geological materials. A complete understanding of point defect mechanisms and how they control diffusion rates even in impure natural crystals allows diffusion coefficients at various conditions to be calculated and compared with experimental measurements. This ensures that errors from erratic measurements of diffusion coefficients or extrapolations do not vitiate diffusion modeling to extract timescales (Chakraborty 2008).
2. It has been recognized that the presence of water in the system of interest can have a significant influence on diffusion in many geologic materials (Watson and Baxter 2007), even in trace amounts. If water is present, water fugacities are an essential part of the experimental data set. Moreover, since hydrogen is an incompatible element for most minerals, it is very likely that it strongly segregates into grain boundaries, profoundly affecting grain-boundary diffusion. However, the effect of H species on diffusion in crystals is less well understood so far.
3. Diffusion in polycrystalline materials may occur rapidly along grain boundaries, crystal interfaces, or surfaces and will not necessarily record intracrystalline diffusivities. Therefore, if polycrystalline materials are used in diffusion experiments

to determine intrinsic or volume diffusion coefficients, then the contributions of extrinsic grain-boundary diffusion must be shown to be negligible.

4. Most systems are thermodynamically nonideal and in addition to a concentration gradient other driving forces such as chemical potential gradients, stress gradients or temperature gradients exist (Chakraborty 2008). Notably, the roles of stress gradients and strain rates in the diffusion experiments have not been investigated yet.

Improvement on the above issues will not only constrain the above issues, but also will impact on our understanding of the thermodynamics, transport, and other physical and chemical properties of the Earth's materials, as well as our understanding of geological and planetary processes.

Acknowledgements This study was supported by the Strategic Priority Research Program (B) of the Chinese Academy of Sciences (XDB 18010401), the 1000Plan Program for Young Talents and Hundred Talent Program of CAS and NSF of China (41303048) to BZ. We gratefully acknowledge the constructive comments of two anonymous reviewers, and the handling editor S.-I. Karato.

References

Ammann MW, Brodholt JP, Wookey J, Dobson DP (2010) First-principles constraints on diffusion in lower-mantle minerals and a weak D″ layer. Nature 465:462–465

Béjina F, Jaoul O (1997) Silicon diffusion in silicate minerals. Earth Planet Sci Lett 153:229–238

Béjina F, Jaoul O, Liebermann RC (2003) Diffusion in minerals at high pressure: a review. Phys Earth Planet Inter 139:3–20

Béjina F, Blanchard M, Wright K, Price GD (2009) A computer simulation study of the effect of pressure on Mg diffusion in forsterite. Phys Earth Planet Inter 172:13–19

Bokshtein BS, Bokshtein SZ, Zhukhovitskii AA (1985) Thermodynamics and kinetics of diffusion in solids. Oxonian Press, New Delhi

Bolfan-Casanova N (2005) Water in the Earth's mantle. Mineral Mag 69(3):229–257

Borg RJ, Dienes GJ (1988) An introduction to solid state diffusion. Academic Press, Boston

Borinski SA, Hoppe U, Chakraborty S, Ganguly J, Bhowmik SK (2012) Multicomponent diffusion in garnets I: general theoretical considerations and experimental data for Fe-Mg systems. Contrib Mineral Petrol 164:571–586

Brady JB (1995) Diffusion data for silicate minerals, glasses, and liquids. In: Ahrens TJ (ed) Mineral physics and crystallography: A handbook of physical constants. AGU, Washington DC, pp 269–290

Brady JB, Cherniak DJ (2010) Diffusion in minerals: an overview of published experimental data. Rev Mineral Geochem 72:899–920

Buening DK, Buseck PR (1973) Fe-Mg lattice diffusion in olivine. J Geophys Res 78:6852–6862

Chakraborty S (1997) Rates and mechanisms of Fe–Mg interdiffusion in olivine at 980°C–1300°C. J Geophys Res 102:12317–12331

Chakraborty S (2008) Diffusion in solid silicates—a tool to track timescales of processes comes of age. Annu Rev Earth Planet Sci 36:153–190

Chakraborty S (2010) Diffusion coefficients in olivine, wadsleyite and ringwoodite. Rev Mineral Geochem 72:603–639

Chakraborty S, Farver JR, Yund RA, Rubie DC (1994) Mg tracer diffusion in synthetic forsterite and San Carlos olivine as a function of P, T and fO_2. Phys Chem Miner 21:489–500

Chakraborty S, Knoche R, Schulze H, Rubie DC, Dobson D, Ross NL, Angel RJ (1999) Enhancement of cation diffusion rates across the 410-kilometer discontinuity in earth's mantle. Science 283:362–365

Cherniak DJ (1993) Lead diffusion in titanite and preliminary results on the effects of radiation damage on Pb transport. Chem Geol 110:177–194

Cherniak DJ, Dimanov A (2010) Diffusion in pyroxene, mica and amphibole. Rev Mineral Geochem 72:641–690

Cherniak DJ, Hervig R, Koepke J, Zhang Y, Zhao D (2010) Analytical methods in diffusion studies. Rev Mineral Geochem 72:107–169

Chiang YM, Birnie DP, Kingery WD (1997) Physical ceramics. Willey Chichester, UK

Crank J (1975) The Mathematics of Diffusion (2nd edition). Oxford University Press, London, pp 1–414

Demouchy S, Mackwell SJ, Kohlstedt DL (2007) Influence of hydrogen on Fe-Mg interdiffusion in (Mg, Fe)O and implications for Earth's lower mantle. Contrib Mineral Petrol 154:279–289
Dimanov A, Sautter V (2000) "Average" interdiffusion of (Fe, Mn)–Mg in natural diopside. Eur J Mineral 12(4):749–760
Dimanov A, Wiedenbeck M (2006) (Fe, Mn)–Mg interdiffusion in natural diopside: effect of pO2. Eur J Mineral 18(6):705–718
Dobson DP, Richmond NC, Brodholt JP (1997) A high temperature electrical conduction mechanism in the lower mantle phase (Mg, Fe)$_{1-X}$O. Science 275:1779–1781
Dohmen R, Chakraborty S (2007) Fe-Mg diffusion in olivine II: point defect chemistry, change of diffusion mechanisms and a model for calculation of diffusion coefficients in natural olivine. Phys Chem Miner 34:409–430
Dohmen R, Becker HW, Chakraborty S (2007) Fe–Mg diffusion in olivine I: experimental determination between 700 and 1200°C as a function of composition, crystal orientation and oxygen fugacity. Phys Chem Miner 34:389–407
Dohmen R, Heege JH, Becker HW, Chakraborty S (2016) Fe–Mg interdiffusion in orthopyroxene. Am Mineral 101:2210–2221
Elphick SC, Ganguly J, Loomis TP (1985) Experimental determination of cation diffusivities in aluminosilicate garnets: I. experimental methods and interdiffusion data. Contrib Mineral Petrol 90:36–44
Farber DL, Williams Q, Ryerson FJ (2000) Divalent cation diffusion in Mg_2SiO_4 spinel (ringwoodite), β phase (wadsleyite), and olivine: implications for the electrical conductivity of the mantle. J Geophys Res 105:513–529
Fei H (2013) Silicon and oxygen self-diffusion in forsterite and implications to upper-mantle rheology. PhD dissertation. University of Bayreuth, Germany
Freer R (1981) Diffusion in silicate minerals and glasses: a data digest and guide to the literature. Contrib Mineral Petrol 76(4):440–454
Freer R, Edwards A (1999) An experimental study of Ca-(Fe, Mg) interdiffusion in silicate garnets. Contrib Mineral Petrol 134(4):370–379
Freer R, O'Reilly W (1980) The diffusion of Fe^{2+} ions in spinel with relevance to the process of maghemitization. Mineral Mag 43:889–899
Ganguly J (2002) Diffusion kinetics in minerals: principles and applications to tectono-metamophic processes. EMU Notes in Mineral 4:271–309
Ganguly J, Tazzoli V (1994) Fe^{2+}–Mg interdiffusion in orthopyroxene: retrieval from the data on intracrystalline exchange reaction. Am Mineral 79:930–937
Ganguly J, Tirone M (1999) Diffusion closure temperature and age of a mineral with arbitrary extent of diffusion: theoretical formulation and applications. Earth Planet Sci Lett 170:131–140
Ganguly J, Cheng W, Chakraborty S (1998) Cation diffusion in aluminosilicate garnets: experimental determination in pyrope–almandine diffusion couples. Contrib Mineral Petrol 131(2):171–180
Hart SR (1981) Diffusion compensation in natural silicates. Geochim Cosmochim Acta 45(3):279–291
Hier-Majumder S, Anderson IM, Kohlstedt DL (2005) Influence of protons on Fe–Mg interdiffusion in olivine. J Geophys Res 110:B02202
Holzapfel C, Rubie DC, Mackwell SJ, Frost DJ (2003) Effect of pressure on Fe–Mg interdiffusion in (Fe_xMg_{1-x})O, ferropericlase. Phys Earth Planet Inter 139:21–34
Holzapfel C, Rubie DC, Frost DJ, Langenhorst F (2005) Fe–Mg interdiffusion in (Mg, Fe)SiO_3 perovskite and lower mantle reequilibration. Science 309:1707–1710
Holzapfel C, Chakraborty S, Rubie DC, Frost DJ (2007) Effect of pressure on Fe–Mg, Ni and Mn diffusion in (Fe_xMg_{1-x})$_2SiO_4$ olivine. Phys Earth Planet Inter 162:186–198
Holzapfel C, Chakraborty S, Rubie DC, Frost DJ (2009) Fe–Mg interdiffusion in wadsleyite: the role of pressure, temperature and composition and the magnitude of jump in diffusion rates at the 410 km discontinuity. Phys Earth Planet Inter 172(1):28–33
Ingrin J, Skogby H (2000) Hydrogen in nominally anhydrous upper-mantle minerals concentration levels and implications. Eur J Mineral 12:543–570
Ito Y, Toriumi M (2010) Silicon self-diffusion of $MgSiO_3$ perovskite by molecular dynamics and its implication for lower mantle rheology. J Geophys Res 115(B12):B12205. doi:10.1029/2010JB000843
Jaoul O, Raterron P (1994) High-temperature deformation of diopside crystal: 3 influences of pO_2 and SiO_2 precipitation. J Geophys Res 99(B5):9423–9439
Jaoul O, Bertran-Alvarez Y, Liebermann RC, Price GD (1995) Fe–Mg interdiffusion in olivine up to 9 GPa at $T = 600$–900°C; experimental data and comparison with defect calculations. Phys Earth Planet Inter 89:199–218
Jones AG (2014) Compensation of the Meyer–Neldel Compensation Law for H diffusion in minerals. Geochem Geophys Geosyst 15:2616–2631

Kohlstedt DL, Keppler H, Rubie DC (1996) Solubility of water in the α, β and γ phases of $(Mg, Fe)_2SiO_4$. Contrib Mineral Petrol 123:345–357
Kubo T, Shimojuko A, Ohtani E (2004) Fe-Mg interdiffusion rates in wadsleyite and the diffusivity jump at the 410 km discontinuity. Phys Chem Miner 31:456–464
Liermann HP, Ganguly J (2002) Diffusion kinetics of Fe^{2+} and Mg in aluminous spinel: experimental determination and applications. Geochim Cosmochim Acta 66:2903–2913
Mackwell SJ, Bystricky M, Sproni M (2005) Fe–Mg interdiffusion in (Mg, Fe)O. Phys Chem Miner 32(5–6):418–425
Mehrer H (2007) Diffusion in solids: fundamentals, methods, materials, diffusion-controlled processes. Springer, Berlin
Misener DJ (1974) Cation diffusion in olivine to 1400°C and 35 kbar. In: Hofmann AW, Giletti BJ, Yoder HS Jr, Yund RA (eds) Geochemical transport and kinetics, vol 634. Carnegie Inst Wash Publ, Washington, pp 117–129
Mueller T, Watson EB, Harrison TM (2010) Applications of diffusion data to high-temperature earth systems. Rev Mineral Geochem 72(1):997–1038
Müller T, Dohmen R, Becker HW, ter Heege JH, Chakraborty S (2013) Fe–Mg interdiffusion rates in clinopyroxene: experimental data and implications for Fe–Mg exchange geothermometers. Contrib Mineral Petrol 166:1563–1576
Otsuka K, Karato S (2015) The influence of ferric iron and hydrogen on Fe–Mg interdiffusion in ferropericlase ((Mg, Fe)O) in the lower mantle. Phys Chem Miner 42(4):261–273
Ringwood AE (1975) Composition and petrology of the earth's mantle. McGraw-Hill, New York, pp 1–618
Shewmon PG (1963) Diffusion in solids. McGraw-Hill, New York
Tachibana S, Tamada S, Kawasaki H, Ozawa K, Nagahara H (2013) Interdiffusion of Mg–Fe in olivine at 1400–1600°C and 1 atm total pressure. Phys Chem Miner 40(6):511–519
Tilley RJD (2008) Defects in solids. Wiley, New York
Van Orman JA, Crispin KL (2010) Diffusion in oxides. Rev Mineral Geochem 72:757–825
Vogt K, Dohmen R, Chakraborty S (2015) Fe–Mg diffusion in spinel: new experimental data and a point defect based model. Am Mineral 100:2112–2122
Wang Z, Hiraga T, Kohlstedt DL (2004) Effect of H^+ on Fe–Mg interdiffusion in olivine $(Fe, Mg)_2SiO_4$. Appl Phys Lett 85:209–211
Watson EB, Baxter EF (2007) Diffusion in solid-Earth systems. Earth Planet Sci Lett 253(3):307–327
Watson EB, Cherniak DJ (2003) Lattice diffusion of Ar in quartz, with constraints on Ar solubility and evidence of nanopores. Geochim Cosmochim Acta 67(11):2043–2062
Xu JS, Yamazaki D, Katsura T, Wu XP, Remmert P, Yurimoto H, Chakraborty S (2011) Silicon and magnesium diffusion in single crystal of $MgSiO_3$ perovskite. J Geophys Res 116:B12205
Yamazaki D, Irifune T (2003) Fe–Mg interdiffusion in magnesiowüstite up to 35 GPa. Earth Planet Sci Lett 216:301–311
Yamazaki D, Karato S (2001) Some mineral physics constraints on the rheology and geothermal structure of Earth's lower mantle. Am Mineral 86(4):385–391
Yoshino T, Ito E, Katsura T, Yamazaki D, Shan S, Guo X, Nishi M, Higo Y, Funakoshi K (2011) Effect of iron content on electrical conductivity of ferro-periclase with implications for the spin transition pressure. J Geophys Res 116:B04202
Zhang Y (2010) Diffusion in minerals and melts: theoretical background. Rev Mineral Geochem 72(1):5–59
Zhang BH (2012) Diffusion of hydrogen in (Mg, Fe)2SiO4 and high pressure polymorphs refined by the cBΩ model. J Asian Earth Sci 54–55:9–17
Zhang BH, Shan SM (2015a) Thermodynamic calculations of Fe–Mg interdiffusion in (Mg, Fe)2SiO4 polymorphs and perovskite. J Appl Phys 117(5):054906
Zhang BH, Shan SM (2015b) Application of the cBΩ model to the calculation of diffusion parameters of Si in silicates. Geochem Geophys Geosyst 16:705–718
Zhang Y, Ni H, Chen Y (2010a) Diffusion data in silicate melts. Rev Mineral Geochem 72(1):311–408
Zhang BH, Wu XP, Xu JS, Zhou RL (2010b) Application of the cBΩ model for the calculation of oxygen self-diffusion coefficients in minerals. J Appl Phys 108(5):053505
Zhang BH, Wu XP, Zhou RL (2011) Calculation of oxygen self-diffusion coefficients in Mg_2SiO_4 polymorphs and $MgSiO_3$ perovskite based on the compensation law. Solid State Ion 186(1):20–28
Zhao ZF, Zheng YF (2007) Diffusion compensation for argon, hydrogen, lead, and strontium in minerals: empirical relationships to crystal chemistry. Am Mineral 92(2–3):289–308
Zheng YF, Fu B (1998) Estimation of oxygen diffusivity from anion porosity in minerals. Geochem J 32:71–89